HAL
open science

A review of segmentation methods in short axis cardiac MR images.

Caroline Petitjean, Jean-Nicolas Dacher

To cite this version:

Caroline Petitjean, Jean-Nicolas Dacher. A review of segmentation methods in short axis cardiac MR images.. Medical Image Analysis, 2010, epub ahead of print. 10.1016/j.media.2010.12.004 . hal-00551034

HAL Id: hal-00551034

https://hal.science/hal-00551034v1

Submitted on 1 Jan 2011

HAL is a multi-disciplinary open access archive for the deposit and dissemination of scientific research documents, whether they are published or not. The documents may come from teaching and research institutions in France or abroad, or from public or private research centers.

L'archive ouverte pluridisciplinaire **HAL**, est destinée au dépôt et à la diffusion de documents scientifiques de niveau recherche, publiés ou non, émanant des établissements d'enseignement et de recherche français ou étrangers, des laboratoires publics ou privés.

A review of segmentation methods in short axis cardiac MR images

Caroline Petitjean[a,*], Jean-Nicolas Dacher[b]

[a] *Université de Rouen, LITIS EA 4108, BP 12, 76801 Saint-Etienne-du-Rouvray, France*
[b] *University Hospital of Rouen, Department of Radiology & University of Rouen, INSERM U644 76031 Rouen, France*

Abstract

For the last 15 years, Magnetic Resonance Imaging (MRI) has become a reference examination for cardiac morphology, function and perfusion in humans. Yet, due to the characteristics of cardiac MR images and to the great variability of the images among patients, the problem of heart cavities segmentation in MRI is still open. This paper is a review of fully and semi-automated methods performing segmentation in short axis images using a cardiac cine MRI sequence. Medical background and specific segmentation difficulties associated to these images are presented. For this particularly complex segmentation task, prior knowledge is required. We thus propose an original categorization for cardiac segmentation methods, with a special emphasis on what level of external information is required (weak or strong) and how it is used to constrain segmentation. After reviewing method principles and analyzing segmentation results, we conclude with a discussion and future trends in this field regarding methodological and medical issues.

Keywords: Cardiac, MRI, Segmentation, Deformable models, Shape prior, Statistical model

1. Introduction

Cardiovascular diseases are the leading cause of death in Western countries (Allender et al., 2008; Lloyd-Jones, 2010). Diagnosis and treatment

*Corresponding author. Tel: +33 232 955 215 - Fax: +33 232 955 022
Email addresses: `Caroline.Petitjean@univ-rouen.fr` (Caroline Petitjean), `Jean-Nicolas.Dacher@chu-rouen.fr` (Jean-Nicolas Dacher)

follow-up of these pathologies can rely on numerous cardiac imaging modalities, which include echography, CT (computerized tomography), coronary angiography and cardiac MRI. Today recognized as a reference modality for the non-invasive assessment of left ventricular function, MRI also supplies accurate information on morphology, muscle perfusion, tissue viability or blood flow, using adequate protocols. The cardiac contractile function can be quantified through ventricle volumes, masses and ejection fraction, by segmenting the left (LV) and right (RV) ventricles from cine MR images. Manual segmentation is a long and tedious task, which requires about 20 minutes per ventricle by a clinician. Because this task is also prone to intra- and inter-observer variability, there has been a lot of research work about automated segmentation methods. In particular, commercial software packages such as MASS (Medis, Leiden, The Netherlands) (van der Geest et al., 1994) and Argus (Siemens Medical Systems, Germany) (O'Donnell et al., 2006) are today available for automatic ventricle delineation. Even though processing time has been greatly reduced, the provided contour detection still needs to be improved to equal manual contour tracing (François et al., 2004; Mahnken et al., 2006). While reviews on cardiac image analysis (Suri, 2000; Frangi et al., 2001) and medical image segmentation (Suri et al., 2001; Pham et al., 2000) exist, we have focused on methods dedicated to cardiac MR segmentation: the particular shape of both ventricles, as well as MR characteristics, have required specific developments. Despite more than 15 years of research, the problem is still open, as shown by the holding of a segmentation contest on the LV in 2009 during the MICCAI conference[1], and remains completely unsolved for the RV.

In the present paper, we will review automatic and semi-automatic segmentation methods of cine MR images of the cardiac ventricles, using the short-axis view, the most common imaging plane to assess the cardiac function. We wish to provide the reader with (i) major challenges linked to this segmentation task, (ii) a state-of-the art of cardiac segmentation methods, including debut methods and current ones, and (iii) future trends in this field. This paper is intended for researchers in the field of cardiac segmentation, but also to image processing and pattern recognition researchers interested

[1]MICCAI Workshop - Cardiac MR Left Ventricle Segmentation Challenge, `http://smial.sri.utoronto.ca/LV_Challenge/`, 2009.

to see how different segmentation techniques apply for a given application. The remaining of the paper is as follows. Short-axis MR images and the challenge of their segmentation are presented in Section 2. In Section 3, a categorization for segmentation methods is proposed and justified. Segmentation methods are presented in Section 4 and their results are discussed in Section 5. At last conclusion and perspectives are drawn in Section 6.

2. Cardiac MR image processing

2.1. Description of short-axis MR images

The complexity of segmenting heart chambers and myocardium mainly relies on heart anatomy and MRI acquisition specificity. The LV function consists in pumping the oxygenated blood to the aorta and consequently to the systemic circuit. The LV cavity has a well-known shape of ellipsoid (Figure 1) and is surrounded by the myocardium, whose normal values for thickness range from 6 to 16 mm. On the contrary, the RV has a complex crescent shape. It also faces lower pressure to eject blood to the lungs and is thus three to six times thinner than the LV, reaching the limit of MRI spatial resolution. For those reasons, and because its function is less vital than the LV's, most research effort has focused on the LV, even though MRI has proven to provide an accurate quantification of RV mass (Shors et al., 2004).

Let us now describe the data that compose a typical cardiac MR examination. The standard imaging plane is perpendicular to the long (apex-base) axis and called short axis plane (Figure 2). Imaging of the heart in MRI covers the whole organ with about 8 to 10 short-axis slices, distance between two adjacent slices ranging from 10 to 20 mm. As the heart is a moving organ, images are acquired throughout the cardiac cycle, thanks to the synchronisation of MR acquisition to the ECG signal and the use of cine (i.e. dynamic) MR sequences. In full-size images, the ventricles cover quite a small surface in cardiac MR images and processing is usually restricted to a smaller region of interest (ROI). About thirty phases (or images) can be obtained during one cardiac cycle with the currently available equipment, yielding a temporal resolution of about 30 ms. The number of phases decreases proportionally to the heart rate. A single examination can thus be made up of 250 images.

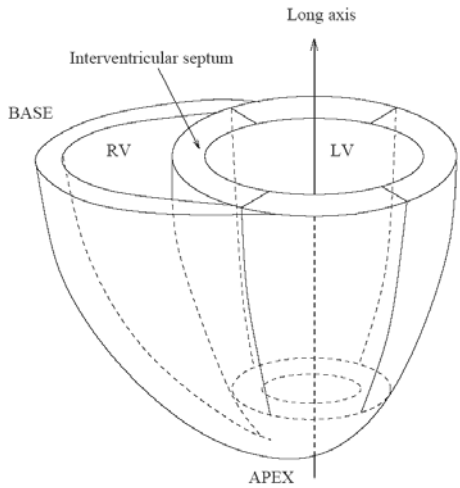

Figure 1: LV and RV geometry

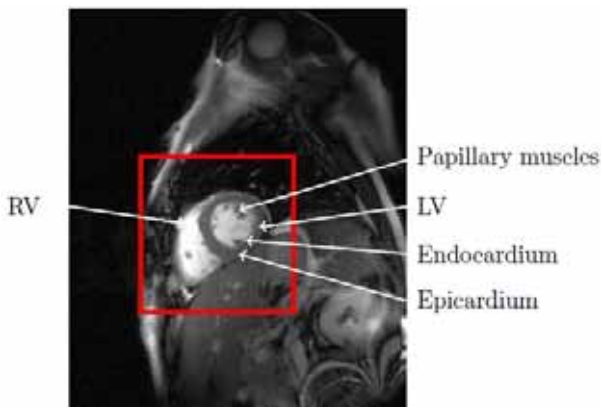

Figure 2: A full size short-axis cardiac MR image and a ROI identifying the heart

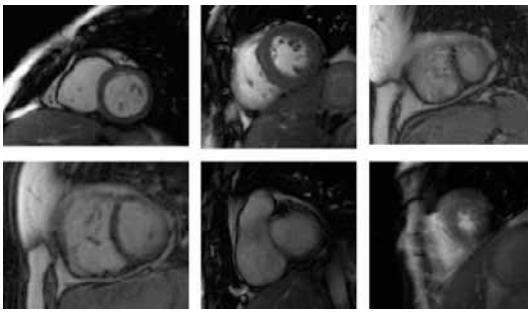

Figure 3: Variability among cardiac images

On a typical MR image (Figure 2), blood pools appear bright and myocardium and surrounding structures appear dark, with a spatial resolution of around 1.5mm per pixel. This aspect is due to the use of balanced Fast Field Echo (bFFE) sequences. These MR sequences have been replacing standard gradient echo for the last 5 years, thus considerably improving image quality. As shown in Figure 3, cardiac MR image exhibit a great variability, be it in terms of gray levels or structure shapes. Gray level intensities can also differ due to the use of different MRI scans or different bFFE sequences. Fuzziness can be observed on some parts of the images, mostly due to blood flow and partial volume effects, aggravated by respiration motion artefacts. This former effect is a consequence of non-zero thickness of MRI slices: in some areas, a voxel can be a mixture of several tissue types. In terms of shape, the ventricle varies over patients, over time and over the long axis. This variability must be accounted for in segmentation algorithms.

2.2. Issues in cardiac MR image segmentation

Segmentation of the heart on these images consists in delineating the outer wall, also called epicardium and the inner wall, called endocardium (Figure 2). Each contour to be delineated presents specific segmentation difficulties, as described below.

Epicardium segmentation The epicardial wall is at the frontier between the myocardium and surrounding tissues (fat, lung), which have different intensity profiles and show poor contrast with the myocardium. Segmentation of the epicardial wall is thus difficult, especially for the RV because

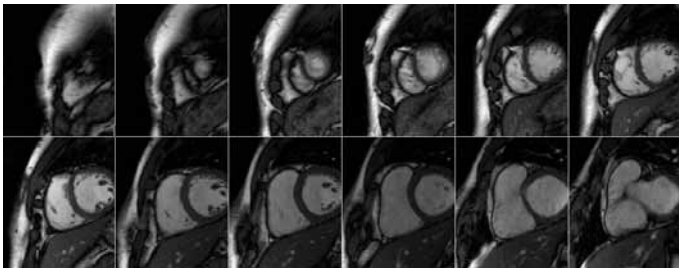

Figure 4: Cardiac images corresponding to 12 short-axis slices from apex to base

of its reduced thickness.

Endocardium segmentation Endocardium surrounds the LV cavity. MRI provides quite good contrast between myocardium and the blood flow without the need of contrast medium. Still segmentation difficulties exist, that mostly originate from gray level inhomogeneities because of blood flow, and particularly because of the presence of papillary muscles and trabeculations (wall irregularities) inside the heart chambers, which have the same intensity profile as the myocardium (Figure 2). They can thus prevent from clearly delineating this wall. According to clinical standards, they should not be taken into account for endocardial wall segmentation. Because the endocardial wall is less difficult to segment that the epicardial one, and since it is the only contour required to compute ventricular volume, some segmentation methods only focus on its segmentation.

Position along the apex-base axis Segmentation complexity also depends on the slice level of the image. Apical and basal slice images are more difficult to segment than mid-ventricular images. Indeed, MRI resolution is not high enough to resolve size of small structures at the apex and ventricle shapes are strongly modified close to the base of the heart, because of the vincinity of the atria. Note also that the RV shape varies much throughout the apex-base axis, whereas the LV remains close to a ring shape, as shown in Figure 4.

2.3. Quantification of cardiac systolic function

Endocardial and epicardial contours are used to quantify the heart function. Physicians are especially interested by the computation of the RV and LV mass and volume at two precise moments of the cardiac cycle: the time

Figure 5: Cardiac MR images at end diastole (left) and end systole (right)

of greatest contraction (end systole, ES) and the time of maximum filling (end diastole, ED) (Figure 5). Volume is obtained by integrating surfaces obtained on the endocardium only, whereas mass computation requires the integration of both endocardial and epicardial surfaces. Volumes at end systole and end diastole are then compared by computing the so-called ejection fraction, defined as the ratio of the difference in heart volume during ED and ES times to the ED time. The computation of clinical parameters thus only requires contours at two instants of the cardiac cycle. Full cycle segmentation of the ventricles, although not used currently in clinical routine, allows to assess temporal volume and mass variations and would be of great interest as an indicator of cardiac performance (Caudron et al., 2011). It also allows to compute endocardial and epicardial wall motion, as well as myocardium thickening. Note that, because of the aperture problem, intramyocardial motion cannot be analyzed from standard cine-MR images but requires dedicated modalities such as tagged MRI (Rougon et al., 2005).

3. Overview of segmentation methods

For this review, we have been considering the papers among peer-reviewed publications, that included (i) a segmentation method for delineating the LV, the RV, or both, (ii) qualitative or quantitive assessment of the method and (iii) illustrations on cardiac MR data. All 70 reviewed papers have been listed in Table 2. Classifying these methods is not a trivial task. A common categorization for medical image segmentation includes thresholding, edge-based and region-based approaches, pixel-based classification, and atlas-guided approaches (Dawant and Zijdenbos, 2000; Pham et al., 2000). In the following section we explain how this categorization can be used with a few nuances and what criteria is chosen to classify the different methods.

3.1. A categorization of short-axis MR image segmentation methods

Numerous segmentation problems require the use of a priori knowledge so as to increase their robustness and accuracy. On one hand, user interaction, an important consideration in any segmentation problem (Pham et al., 2000), can be regarded as a priori knowledge. In our application, it can consist in pointing the center of the LV cavity or manually tracing the ventricle border. These two levels of user interaction do not have the same impact in terms of reproductibility, neither require the same level of expertise, and are thus going to be distinguished. On the other hand, as medical expertise is available on cardiac ventricles, it can be used during the segmentation process, with different levels of information as well. Prior information can consist in weak assumptions such as simple spatial relationships between objects (for instance, the RV is to the left of the LV) or anatomical assumptions making use of the circular geometry of the LV. The knowledge of the heart biomechanics can also be integrated into the segmentation process, to constrain adequately the segmentation of the different phases. More accurate information regarding the shape of the heart can also be obtained through higher-level information, such as a statistical shape model. On some images, especially at the apex, myocardium borders are very fuzzy and ill-defined, and it is very difficult to rely on the image alone to perform segmentation. The use of a shape model for example is thereby particularly useful, but at the expense of building a training data set with manually generated segmentations. We will thus distinguish three main levels of information used during the segmentation process: (i) no prior, (ii) weak prior, that includes anatomical and biomechanical models, or (iii) strong prior. In this review, we shall see how the level of information used is correlated to the type of segmentation method and the level of user interaction.

Image-driven techniques, such as thresholding, region-based or edge-based techniques, or else pixel classification, offer a limited framework for strong prior incorporation. Deformable models, including snakes and their variants, on the contrary, offer a great, versatile framework for using either weak or strong prior. They can include geometrical information, as well as high level information, in the so-called shape prior based segmentation framework, or through active shape models (ASM) and active appearance models (AAM). At last, atlas guided segmentation also make use of a set of manually segmented images. Considering both the usual segmentation method categorization and the level of external information, we propose the following two

Table 1: Categorization of segmentation methods vs. type of prior information and related sections in the paper

	Region- and edge-based	Pixel Classification	Deformable models	ASM/AAM	Atlas
No prior	Section 4.2.1.	Section 4.2.2.	Section 4.2.3.		
Weak prior					
Strong prior			Section 4.3.1.	Section 4.3.2.	Section 4.3.3.

main categories (Table 1):

- segmentation based on no or weak prior, that includes image-based and pixel classification based methods, as well as deformable models ;
- segmentation based on strong prior, that includes shape prior based deformable models, active shape and appearance models, and atlas based methods.

Methods combining strong and weak priors have been categorized in the strong prior section. In the next section, comparison criteria for segmentation methods are detailed.

3.2. Points of comparison for segmentation methods

Segmentation methods are compared in Table 2, on the basis of their experimental conditions. Notations and acronyms used in this table are explained below.

LV/RV This flag indicates whether segmentation results are provided on both LV (resp. RV) epicardial and endocardial contours (LV, RV), or endocardial only (LVv, RVv).

User interaction (U) User interaction may be used for segmentation initialization. We will distinguish between limited user interaction (U1), such as pointing the LV center or dragging a circle, and advanced user interaction (U2), that consists in manually segmenting the first image of the sequence. When no user interaction is needed, most methods start with an automatic localization of the heart (A). Methods for which no user interaction nor automatic heart localization is reported are specified with a hyphen (-).

Use of external information (E) External information incorporated during the segmentation process may be a weak prior, that can be based on anatomical modeling (AM) such as (i) the circular aspect of the LV: transformation into polar coordinates, use of radial lines, (ii) simple spatial relationships, e.g. the RV is positioned on the left side of the LV, or (iii) the use of an ellipsoid, cylinder or bullet-shaped volumetric model. Assumptions based on heart motion and deformations, such as the fiber stiffness, can be integrated into a biophysical model (BM). A strong prior (SP), namely a set of manually drawn borders gathered and synthetized into a statistical model, may also be used. Methods making no use of external information at all are specified with a hyphen (-).

Use of motion information (M) As the heart is a moving organ, its motion can be taken into account in the segmentation process. We are not interested in the underlying contour point tracking problem, that would consist in recovering the trajectories of material points, but rather by how the time dimension can help the segmentation process (Montagnat and Delingette, 2005). We will distinguish between approaches that propagate an initial segmentation result (P) on the whole cardiac cycle by repeating their algorithm on each image, and approaches that explicitely take motion into account (M). Methods that do not make use of heart motion at all are specified with a hyphen (-).

Assessment of segmentation accuracy (ASA) The performance of segmentation method is quantified through validation against a ground truth. Gold standard in this domain is manual delineation by an expert. Although qualitative visual evaluation is sometimes provided in certain studies (specified with a hyphen), segmentation accuracy is usually assessed by computing and comparing quantitative measures such as ventricle surface (S), volume (V) and mass (M), and ejection fraction (EF) based on contours obtained manually and automatically. Note that because of error compensation, these measures do not totally ensure accurate segmentation results. In order to compare contours (resp. surfaces), accuracy is better estimated by computing the mean perpendicular distance between them, denoted as point-to-curve (P2C) error (resp. point-to-surface (P2S) error). Correlation between manual tracing and automatic method, as well as inter-expert variability may be estimated through linear regression and Bland-Altman analysis. This latter analysis allows for comparison between two measurements by plotting

the difference between the two measurements against their mean (Bland and Altman, 1986).

We shall now review segmentation methods and explain how issues presented in Section 2.2 are handled, with a first focus on how the heart is roughly localized in the MR image.

4. Ventricle segmentation in cardiac MRI

4.1. Automatic localization of the heart

As mentioned above, a ROI centered on the heart is generally extracted from the original MR image, in order not to process the whole image, thus decreasing computational load. Automatic approaches are twofold: time-based approaches, that take advantage of the fact that the heart is the only moving organ in the images, or object detection techniques. They both have in common the use of the Hough transform, that allows to detect the position of the LV thanks to its circular aspect. Note that works presented in (Cocosco et al., 2004; Huang et al., 2007; Jolly, 2008) are entirely devoted to this preliminary step, highlighting its importance.

When using time dimension, a difference or a variance image can be computed over all the data. In (Pednekar et al., 2006), a difference image is computed between two images where the heart is the largest, i.e. in basal slices of the LV and during end diastole. The resulting image contains a circular region around the LV boundaries, which is detected thanks to a Hough transform. Image difference is also used in (Huang et al., 2007) followed by texture analysis and k-means clustering to isolate heart region. Works proposed in (Cocosco et al., 2004; Gering, 2003) rely on variance computation. Starting from a 3D+t original image, variability along the time dimension is computed with standard deviation of each voxel. The maximum intensity of this resulting 3D image is projected onto a 2D image, binarized using Otsu's method (Otsu, 1979), and dilated several times. The convex hull of the finally obtained region is the final 2D ROI (Figure 6). Some authors found that variance image can be quite noisy and have thus proposed a method based on a Fourier analysis of the image (Lin et al., 2006; Jolly, 2008). A pixelwise Fourier transform of the image sequence over time provides an image of moving structures. Since the heart is the only moving organ in an MR

Table 2: Overview of cardiac MR segmentation methods presented in 70 papers. LV/RV: Left and/or right ventricle segmentation, U: User interaction, E: External information, M: Motion information, ASA: Assessment of segmentation accuracy. Please refer to the text (Section 3.2) for other acronym meaning.

		Authors	Basic method principle	LV/RV	U	E	M	ASA
Segmentation with weak or no prior (47)	Image-based	Gupta et al. (1993)	DP	LV	U2	AM	P	-
		Geiger et al. (1995)	DP	LV	U2	-	P	-
		van der Geest et al. (1994)	DP	LV	U1	AM	P	EF V M
		Goshtasby and Turner (1995)	Thresholding	LVv RVv	A	AM	-	S
		Kaushikkar et al. (1996)	Thresholding	LVv	U1	-	-	EF V
		Weng et al. (1997)	Thresholding	LVv RVv	U1	-	-	-
		Nachtomy et al. (1998)	Thresholding	LV	U1	AM	-	EF V M
		Waiter et al. (1999)	Gradient	LV	U1	-	-	EF
		Lalande et al. (1999)	DP	LV	U1	AM	-	V
		Fu et al. (2000)	DP	LV	U1	-	-	P2C
		Cassen et al. (2001)	Split and merge	LV	U2	-	P	V
		Noble et al. (2003)	Non rigid registration	LV	U2	-	P	EF V
		Yeh et al. (2005)	DP	LVv	U1	AM	-	V
		Liu et al. (2005)	DP	RVv	-	AM	-	-
		Uzümcü et al. (2006)	DP	LV	U2	-	M	EF V P2C
		Katouzian et al. (2006)	Thresholding	LV RVv	U1	-	-	S
		Lin et al. (2006)	Thresholding	LVv	A	AM	P	P2C
		Lee et al. (2008)	Graph searching	LV	U1	AM	-	EF V M
		Jolly et al. (2009)	Shortest path and minimum surf.	LV	A	AM	P	S P2C
		Cousty et al. (2010)	MM, watershed transform	LV	U1	AM	M	EF M P2S
	Pixel classif.	Boudraa (1997)	Clustering (FCM)	LVv	-	AM	-	EF
		Stalidis et al. (2002)	Neural networks	LV	U1	-	M	P2S
		Gering (2003)	GMM, MRF	LV RVv	A	AM	-	-
		Lynch et al. (2006a)	Clustering (K-Means)	LV	-	AM	-	EF S P2C
		Kedenburg et al. (2006)	Fuzzy kNN and graphcut	LV	A	AM	-	V
		Pednekar et al. (2006)	GMM and DP	LV	A	AM	P	EF V
		Cocosco et al. (2008)	Clustering	LVv RVv	A	AM	-	EF V
	Deformable models	Ranganath (1995)	Active contours	LVv	U1	-	P	EF S
		Chakraborty et al. (1996)	Active contours + region term	LV	U1	-	-	-
		Yezzi et al. (1997)	GAC	LV	U1	-	-	V
		Pham et al. (2001)	3D deformable surfaces + GVF	LV	U1	BM	P	V
		Paragios (2002)	GAC + GVF + region term	LV	U1	AM	-	-
		Zhukov et al. (2002)	3D deformable surfaces	LV	U1	AM	-	-
		Papademetris et al. (2002)	Shape based matching	LV	U1	BM	P	-
		Santarelli et al. (2003)	Active contours + GVF	LV	U2	-	P	V M
		Battani et al. (2003)	GAC	RVv	U1	-	-	V
		Pluempitiwiriyawej et al. (2005)	Active contours + region term	LV RV	U1	AM	P	S
		Heiberg et al. (2005)	3D Active contours	LV	U1	AM	P	V
		Wang and Jia (2006)	Active contours + GVF	LV	U1	AM	P	P2C
		Jolly (2006)	GMM + Active contours + splines	LV	U1	AM	P	P2C
		Hautvast et al. (2006)	Discrete active contours	LV RVv	U2	-	P	EF,V P2C
		Gotardo et al. (2006)	Active contours + Fourier desc.	LV	U1	-	P	-
		Sermesant et al. (2006)	Registration	LV RV	U2	BM	P	-
		Yan et al. (2007)	Registration	LV RV	U2	BM	P	-
		El Berbari et al. (2007)	MM + Active contours + GVF	LV	U1	AM	-	S P2C
		Lynch et al. (2008)	Level sets + temporal def. model	LV	A	AM	M	P2C
		Billet et al. (2009)	Deformable models	LV RV	U2	BM	P	-
		Ben Ayed et al. (2009)	Level sets + overlap priors	LV	U2	AM	-	S
Segmentation with strong prior (22)	Shape prior	Paragios et al. (2002)	Level sets and stochastic repres.	LV	-	SM	-	-
		Tsai et al. (2003)	PCA and energy min.	LVv	-	SM	-	-
		Kaus et al. (2004)	PCA and energy min.	LV	-	SM	-	P2S
		Sénégas et al. (2004)	Fourier desc. + Bayesian approach	LV RVv	-	SM	M	P2C
		Sun et al. (2005)	PCA + Bayesian approach	LV	U2	SM	M	-
		Lin et al. (2005)	Probabilistic map + Graphcut	LV	-	SM	-	P2C
		Lynch et al. (2006b)	Level sets + PDF	LV	U1	SM	-	S P2C
	ASM/AAM	Mitchell et al. (2000)	AAM	LV	A	SM	-	P2C
		Stegmann et al. (2001)	AAM	LV	-	SM	-	S P2C
		Mitchell et al. (2001)	Hybrid ASM/AAM	LV RVv	A	SM	-	S P2C
		Lelieveldt et al. (2001)	2D+time AAM	LV	A	SM	M	S P2C
		Mitchell et al. (2002)	3D AAM	LV	A	SM	-	V M P2C
		Ordas et al. (2003)	ASM with IOF	LV RV	-	SM	-	P2C
		Stegmann and Pedersen (2005)	3D bi-temporal AAM	LV	-	SM	-	EF V
		van Assen et al. (2006)	3D ASM	LV	-	SM	-	V P2C
		Abi-Nahed et al. (2006)	ASM + Robust Point Matching	RVv	-	SM	-	P2C
		Zambal et al. (2006)	2D AAM + 3D ASM	LV	-	SM	-	P2S
		Zhang et al. (2010)	AAM + ASM	LV RVv	U2	SM	-	V M P2S
	Atlas	Lorenzo-Valdés et al. (2002)	Anatomical atlas + NRR	LV RVv	-	SM	P	V
		Lorenzo-Valdés et al. (2004)	Probabilistic atlas + EM + MRF	LV RVv	-	SM	P	V P2C
		Lötjönen et al. (2004)	Probabilistic atlas + NRR	LV RV	-	SM	-	P2S
		Zhuang et al. (2008)	Anatomical atlas + NRR	LV RVv	-	SM	-	V P2C

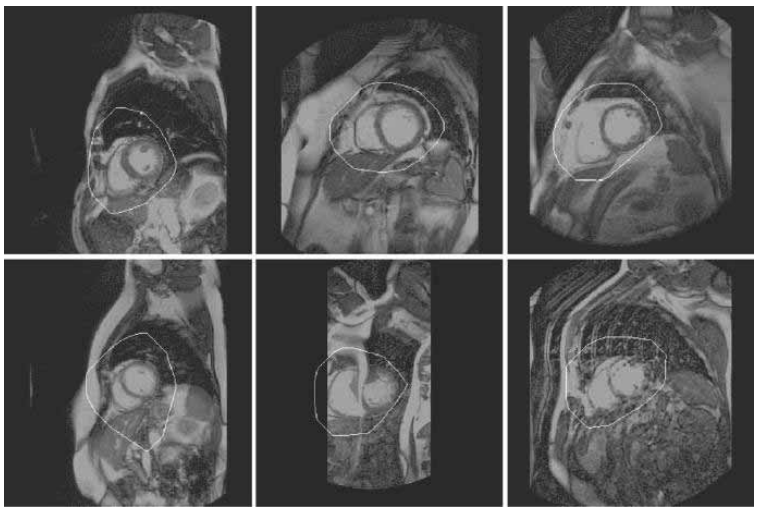

Figure 6: Automatic computed ROI from six patients (from (Cocosco et al., 2004), with kind permission from Elsevier)

image, processing of the first harmonic image allows for localizing the heart.

Contrary to time-based approaches that solely rely on the MR dataset, object detection techniques require a learning stage. Their principle is to extract rectangular subwindows from the image, to compute subwindow features, and to train a classifier to accept the ones containing the heart and reject the rest. The key point lies in the feature extraction step. In (Jolly et al., 2001), it consists in sampling 4 radial intensity profiles centered on the subwindow, and concatenating their gray levels. This global profile is modeled using a Markov chain. The system is trained using positive and negative examples. The detection stage provides a cluster of pixels classified as left ventricle and the final choice among these candidates is made using a Hough based voting procedure on the individual profiles, allowing for sketching a circle roughly positionned on the LV. The method proposed in (Pavani et al., 2010) is based on a popular face detection approach (Viola and Jones, 2001), that consists in a Haar description of the subwindows and a cascade of adaboosted classifiers. Authors suggest to optimize Haar-like features for a given object detection problem by assigning optimal weights to its different Haar basis functions.

4.2. Segmentation with weak or no prior

This section gathers segmentation methods with weak or no prior, including image-based, pixel classification-based and deformable models.

4.2.1. Image-based methods

As seen in Section 2.2, endocardial and epicardial contours present specific segmentation difficulties. Image-based methods propose to process them differently and separately, hence the focusing of certain methods on the LV endocardium only. The first step consists in finding the endocardial contour, usually with thresholding (Goshtasby and Turner, 1995; Weng et al., 1997; Nachtomy et al., 1998; Katouzian et al., 2006) and/or dynamic programming (DP)(Gupta et al., 1993; van der Geest et al., 1994; Geiger et al., 1995; Lalande et al., 1999; Fu et al., 2000; Yeh et al., 2005; Liu et al., 2005; Üzümcü et al., 2006). DP applied to image segmentation consists in searching for the optimal path in a cost matrix that assigns a low cost to object frontiers. Here, the circular geometry of the LV is taken advantage of using polar coordinates, so as to make the search problem one-dimensional. The design of the cost matrix, which is the main difficulty in this problem, can be based on thresholding (van der Geest et al., 1994; Liu et al., 2005), fuzzy logic (Lalande et al., 1999), gray levels, using wavelet-based enhancement (Fu et al., 2000) or radial lines (Yeh et al., 2005), or on the gradient values, used in (Cousty et al., 2010) to weight a spatio-temporal graph. In Jolly et al. (2009), a shortest path algorithm is applied on an image obtained by averaging all the phases over one cardiac cycle, and contours in each individual image are recovered using minimum surface segmentation.

Several solutions are proposed, in order not to include papillary muscles: computation of the convex hull of the contour (van der Geest et al., 1994; Lin et al., 2006), applications of mathematical morphology (MM) operations such as opening and closing on the contour (Nachtomy et al., 1998; Cousty et al., 2010), or fitting a parametric curve to the contour, allowing it to be smooth (Waiter et al., 1999). The epicardium is found during a second step, often relying on the endocardial contour, that makes use of a spatial model incorporating myocardial thickness or MM operators, applied on the endocardial contour. Note that for their initialization, most of these methods rely on a simple user intervention, such as pointing the center of the LV or dragging circles next to the myocardium contours.

When contours are processed identically, the segmentation process is initialized with manually drawn borders on the first image (Cassen et al., 2001; Noble et al., 2003; Üzümcü et al., 2006). Manual contours are then propagated through all subsequent images, using split-and-merge (Cassen et al., 2001), non-rigid registration (Noble et al., 2003), or multidimensional DP: in (Üzümcü et al., 2006) the initial contours provided by the user are resampled to 32 landmarks. Each sample is tracked separately over time by defining a search space around each landmark. Cost hypercubes are then filled with image-feature derived cost function values. The optimal connected path is tracked through cost hypercubes using DP.

4.2.2. Pixel classification based methods

In medical image segmentation, pixel classification is mostly used when multiple images of the same scene are available, as for instance with multispectral MRI or multimodality imaging, e.g. PETscan images (Dawant and Zijdenbos, 2000). Each voxel can be described by several complementary features, and is considered as an item to be classified into a single class among several. The image is partitioned into regions or classes, composed of pixels that have close feature values, using either supervised techniques (with learning samples) or unsupervised ones. In our application, features are usually gray level values and segmentation is mostly performed using two standard unsupervised techniques which are Gaussian Mixture Model (GMM) fitting and clustering. During the segmentation process, methods use geometrical assumptions regarding the location of the ventricle, in order to compensate the lack of spatial information, inherent to classification based methods, but do not require user interaction in general. As for image-based methods, both contours may be processed differently, as shown below.

The principle of GMM is to fit the image histogram with a mixture of gaussians using the Expectation-Minimization (EM) algorithm (Dempster et al., 1977). The number of gaussians, that corresponds to the number of modes in the histogram, must be fixed a priori. Usually, between two and five modes corresponding to encountered tissue types (myocardium, fat, background, blood pool for example) are chosen. Partial volume effect may be accounted for by adding gaussians representing partial voluming between myocardium and blood, myocardium and air (Pednekar et al., 2006). Papillary muscles can be taken into account by assigning a mixture of two gaus-

sians to the ventricle cavity: the blood pool and the myocardium (Sénégas et al., 2004). The EM algorithm can be initialized by using the preliminary step of heart localization (Pednekar et al., 2006) or using an atlas ((Lorenzo-Valdés et al., 2004), see Section 4.3.3). The EM segmentation result can be embedded in a cost matrix for dynamic programming (Pednekar et al., 2006), or precedes a step based on Markov Random Fields (MRF) in order to incorporate spatial correlations into the segmentation process (Gering, 2003). The clustering approach consists in aggregating data in clusters in a feature space. Clustering can be performed through K-means algorithm (Lynch et al., 2006a) or fuzzy C-means, a generalization of K-means allowing partial membership in classes (Boudraa, 1997). After obtaining separate cluster regions, the LV cavity is identified by computing the distance to a circle (Lynch et al., 2006a). The closest blood pool being the one of the RV, the wall between these two cavities is measured to assess the myocardium thickness, which acts as a guide for segmenting the epicardium, using edge information. The epicardium contour is closed using a spline.

Only a few supervised approaches have been proposed, since they require a tedious learning phase, that consists in providing the algorithm with gray levels of labeled pixels. It can be performed by the user, who is required to click on a few sample pixels belonging to myocardium, blood and lung (Stalidis et al., 2002). Theses samples are provided to a generating-shrinking neural network, combined with a spatiotemporal parametric modeling. In this work, the epicardial boundary is found through a radial search, using the previously defined endocardial model. Another possibility is to use a spatial mask applied onto the image, that automatically provides tissue sample to a k-nearest neighbor algorithm, from which a cost map is computed for graphcut segmentation (Kedenburg et al., 2006).

4.2.3. Deformable models

Deformable models have been made popular through the seminal work by Kass et al. (Kass et al., 1988), who introduced active contours, or snakes. Thanks to their flexibility, active contours have been widely used in medical image segmentation (Xu et al., 2000). There are iteratively deforming curves according to the minimization of an energy functional, comprising a data-driven term, that provides information about object frontiers and a regularization term, that controls the smoothness of the curve. This energy

functional is minimized by implementing the Euler-Lagrange equations in a partial differential equation (PDE). In problems of curve evolution, the level set framework has been widely used because it allows for topological changes (Osher and Sethian, 1988). It consists in considering the deforming contour as the zero level of a higher-dimensional function. This implicit representation of the contour allows in particular the segmentation of multiple objects (Caselles et al., 1993). Deformable models have widely been applied to the ventricle segmentation problem either in the parametric framework or in the implicit one using level sets (Yezzi et al., 1997; Battani et al., 2003).

In most of the studies, the regularization term does not change much and is often curvature-based. The contributions regarding ventricle segmentation using deformable models have mainly dealt with the design of the data-driven term. Initially gradient-based (Gupta et al., 1993; Ranganath, 1995; Geiger et al., 1995) and thus sensitive to noise, region-based terms have been introduced, that are based on a measure of region homogeneity (Paragios, 2002; Pluempitiwiriyawej et al., 2005; Chakraborty et al., 1996). In (Ben Ayed et al., 2009), the authors take into account the intensity distribution overlap that exists between myocardium and cavity, and background and myocardium, and introduce a functional that measures how close the overlaps are to a segmentation model, manually obtained in the first frame. The Gradient Vector Flow (GVF) has also been widely used (Xu and Prince, 1998). Initially designed to pull the contour into the object concavities, the GVF consists in diffusing the gradient of an edge map. Authors have noticed that it increases efficiency regarding initialization and convergence, hence its wide use (Pham et al., 2001; Santarelli et al., 2003; Wang and Jia, 2006; El Berbari et al., 2007). Other energy terms have been introduced: in particular, Paragios proposes a coupled propagation of the epicardial and endocardial contours that combines both GVF and level sets (Paragios, 2002) (Figure 7). The relative positions of the endocardium and the epicardium are constrained inside the process. In order to ensure the smoothness of the contour, a parametric shape model (circle, elliptic, spline), e.g. the direct Fourier parameterization of the contour (Staib and Duncan, 1992) allows for compact representation, and easing the formulation of energy (Chakraborty et al., 1996; Gotardo et al., 2006). Note that contour initialization, a crucial step with deformable models, can be carried out through image preprocessing, such as MM operations (El Berbari et al., 2007) or the EM algorithm (Jolly, 2006), or else user interaction, as shown in Table 2.

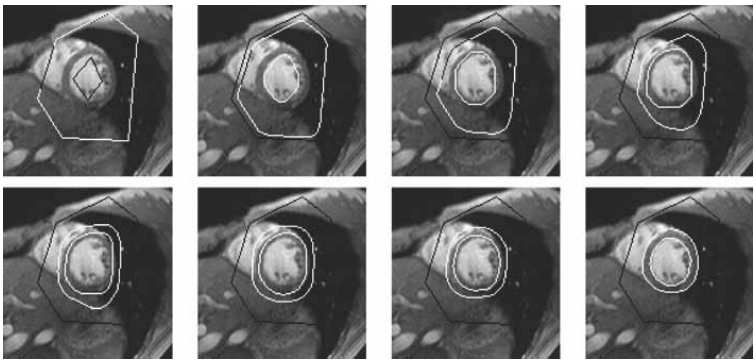

Figure 7: Deformable models and anatomical constraints for the segmentation of the left ventricle. Black contours: initial conditions (from (Paragios, 2002), with kind permission from Springer Science+Business Media.)

Deformable models offer a great framework for 3D extension (Pham et al., 2001; Zhukov et al., 2002; Montagnat and Delingette, 2005; Heiberg et al., 2005)[2], thanks to 3D mesh models, but also to obtain ventricle contours throughout the entire cardiac cycle. A first approach to temporal extension is to apply the segmentation result obtained on the image at time t on the following phase image at time $t + 1$. Whereas it has the advantage of low complexity, this sequential approach does not integrate motion information and does not really exploit the temporal aspect of heart motion. Recent approaches have been developped, that apply constraints on temporal evolution of the contour or surface points: it can be a weak constraint such as averaging point trajectories or a strong constraint such as encoding prior knowledge about cardiac temporal evolution (Montagnat and Delingette, 2005; Lynch et al., 2008) or use a segmentation/registration coupled approach (Paragios et al., 2002).

Volumetric modeling is particularly useful for tracking the LV cavity over time, using a biomechnical model to constrain the segmentation (Pham et al., 2001; Papademetris et al., 2002; Sermesant et al., 2006; Yan et al., 2007; Billet et al., 2009; Casta et al., 2009). The LV myocardium is modeled as a linear

[2]The authors have made their software freely available for research purposes at `http://segment.heiberg.se/` (Heiberg et al., 2010).

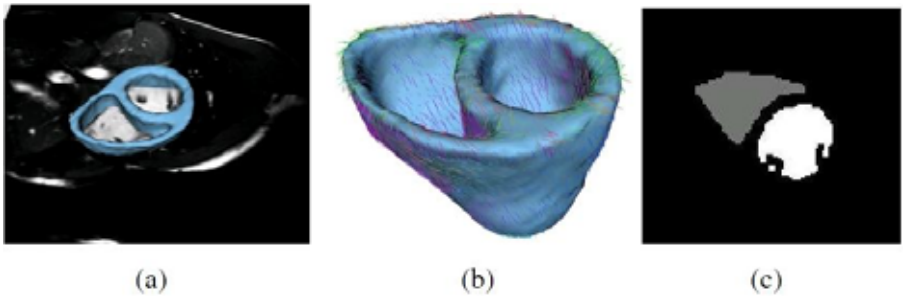

Figure 8: (a) Mid-diastole image. (b) Segmented mesh with synthetic fiber directions. (c) Segmented blood pools of one MR image of the cardiac cycle (from (Billet et al., 2008)).

elastic material defined by several parameters (Poisson's ratio and Young's modulus, or equivalently Lamé's constants), integrated into the so-called stiffness matrix, that defines the material properties of the deforming body in three dimensions. (Pham et al., 2001; Papademetris et al., 2002). The contractility of the myocardium is linked to the muscle fiber directions, which is not isotropic. Fiber orientation can be taken into account by considering different stiffness values for the different material axes (Papademetris et al., 2002). In (Billet et al., 2009), the fiber orientation is part of an electromechanical model, that simulates the cardiac electrophysiology. This model is used to regularize the deformations of the volumetric model. This volumetric meshing is usually initialized with 2D contours manually obtained on the first phases. The mesh is then deformed using an image force and an internal force derived from the biomechanical model as the regularizing term. Segmentation over the whole cardiac cycle is then obtained by minimizing an energy that couples the volumetric deformable model and the image data (Figure 8). The dynamic law of motion expressed in partial diffentiel equations can be solved using finite element method (Pham et al., 2001; Papademetris et al., 2002; Sermesant et al., 2003). Note that these approaches generally include further investigations regarding cardiac motion estimation, tissue deformation analysis and strain computation from 3D image sequences. In particular, the introduction of heart functional information can help recover tangential motion of the ventricle, which cannot be obtained from standard tracking approaches because of the aperture problem (Billet et al., 2009).

4.2.4. Conclusion

A wide variety of image-driven approaches using weak or no prior have been proposed to tackle the ventricle segmentation in cardiac MRI. Almost all of these methods require either minimal or great user intervention. If image-based and pixel classification-based approaches offer a limited framework for incorporating strong prior, straightforward extensions of deformable models in this sense have been extensively studied. In the next section are presented methods relying on strong prior for heart segmentation.

4.3. Segmentation with strong prior

As shown by the growing literature on this matter, automatic organ segmentation can benefit from the use a statistical model regarding shape and/or gray levels, to increase its robustness and accuracy. This especially applies if the nature of the shape does not change much from an individual to another, which is typically the case for the heart. Statistical-model based segmentation techniques comprise three steps:

1. Spatial (and temporal if required) alignment of manually segmented contours or images is of utmost importance to compensate for differences in ventricle position and size, and can be very difficult, especially in 3D (Frangi et al., 2002). One subject in the database is arbitrarily chosen as reference. Every other subject is affinely registered on the reference, and an average shape is computed. This procedure can be performed iteratively by replacing the reference subject with the mean model. When segmentation is computed over the complete cardiac cycle, temporal alignement is needed as well: the number of phases of each individual must be aligned on the number of phases of the reference and thus requires resampling and interpolation (Figure 9).
2. Model construction generally implies the computation of an average shape or image and the modeling of variability present in the training images and contours. This latter can be made via the widely used principal component analysis (PCA), when point correspondences between contour points are available, or else via variance computation or probability density modeling. The PCA provides the eigenvalue decomposition of the shape set covariance matrix, yielding principal eigenvectors (or components), that account for as much of the variability in the data as possible. Each instance of a new shape can thus be described as the mean shape and a weighted linear combination of eigenvectors.

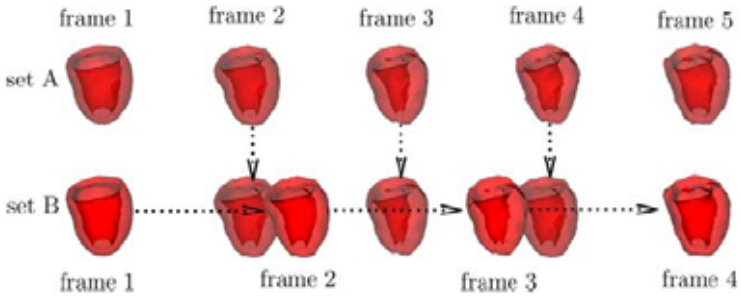

Figure 9: Temporal registration and resampling: linear interpolation is used to generate time frames from image sequence B which correspond to those of sequence A (from (Lorenzo-Valdés et al., 2004), with kind permission from Elsevier)

3. The use of the model for segmentation specifies how the average model is applied to fit the contours in a new image, while taking into account the variability present in the training set.

Methods based on a statistical model mainly fall into three categories: shape prior segmentation (Cremers et al., 2007), active shape and appearance models (Heimann and Meinzer, 2009) and atlas-based segmentation techniques (Rohlfing et al., 2005). Whereas step 1 and 2 are globally common to these methods, they mostly differ by step 3, i.e. the application of the model for segmentation.

4.3.1. Deformable models based segmentation using strong prior

The principle of deformable models with strong prior takes up the variational framework defined in Section 4.2.3. The principle is to modify the energy functional to be minimized by introducing a new term, that embeds an anatomical constraint on the deforming contour, such as a distance to a reference shape model. To construct the reference model, an original variational technique to compute the mean signed distance map is proposed in (Paragios et al., 2002). Then an aligment transformation to this reference is incorporated into the criterion to be minimized. A probability density function (PDF) or probabilistic map can be computed from the data by adding the binary segmented images of both contours, after scaling and alignment. This PDF is embedded as a multiplicative term in the evolution equation (Lynch et al., 2006b) or integrated into the energy function of a graphcut Lin et al. (2005). An alternative to the use of a PDE is proposed in (Tsai

et al., 2003; Kaus et al., 2004), with the advantage of being fast and direct, based on a preliminary PCA on the training data. For a new contour to be segmented, eigenvector weights as well as pose parameters are iteratively updated with a gradient descent, by minimizing the region-based energy terms. Note that these approaches include the coupled propagation of both contours described in Section 4.2.3, that maintains the relative positions of the endocardium and the epicardium according to a distance model (Kaus et al., 2004; Lynch et al., 2006b; Paragios et al., 2002).

To address the temporal aspect of segmentation, approaches relying on bayesian formulation are proposed (Sénégas et al., 2004; Sun et al., 2005). Under the statistical modeling of the image, the segmentation process becomes a MAP (Maximum A Posteriori) estimation. Here, the regularity term is based on the prior, that contains a shape model and a motion model, thus allowing to track ventricle contour over time. The shape model is obtained from an PCA (Sun et al., 2005) or based on a Fourier representation, whose parameters are learned on a database of segmented images (Sénégas et al., 2004). Segmentation is performed with Monte-Carlo techniques or particle filtering.

4.3.2. Active shape and appearance models

The ASM consist of a statistical shape model, called Point Distribution Model (PDM), obtained by a PCA on the set of aligned shapes, and a method for searching the model in an image (Cootes et al., 1995). Segmentation is performed by placing the model on the image, and iteratively estimating rotation, translation and scaling parameters using least square estimation, while constraining the weights of the instance shape to stay within suitable limits for similar shapes. ASM have been extended to gray level modeling, yielding Active appearance models (AAM) (Cootes et al., 1998), that represent both the shape and texture variability seen in a training set. This technique ensures to have a realistic solution, since only shapes similar to the training set are allowed.

AAM applied to LV segmentation are first presented independently in (Mitchell et al., 2000) and in (Stegmann et al., 2001), demonstrating the clinical potential of the approach for the segmentation of both the endocardium and epicardium. Strengths of AAM and ASM can be combined in a hybrid model (Mitchell et al., 2001; Zambal et al., 2006; Zhang et al.,

2010). In (Mitchell et al., 2001), the authors introduce a multistage hybrid model, arguing that AAM are optimized on global appearance but provide imprecise border locations, whereas ASM have a great ability to find local structures. They thus propose to concatenate several independant matching phases, starting with an AAM early stage, that positions the model onto the heart, followed by a hybrid ASM/AAM stage, that allows for position refinement. A final stage of AAM aids in escaping a possible local minimum found during the ASM/AAM stage. Although this method provides accurate results, and, for the first time with AAM, results on the RV, the current model training has been limited to mid-ventricular, end-diastolic images[3]. The idea of combining AAM and ASM has also been used in (Zambal et al., 2006), where the global model construction consists in interconnecting a set of 2D AAMs by a 3D shape model. The goal of the AAM is to match contours on each image individually, while the 3D shape model provides an overall consistency to the instance of the model. The obtained segmentation result is improved on apical slices: if the local matching of 2D AAM fails, is it corrected by the 3D model, through iterative global and local matching.

Several modifications of the original framework have been proposed to increase segmentation accuracy such as the use of an Independent Component Analysis instead of a PCA (Üzümcü et al., 2003), the introduction of ASM with Invariant Optimal Features (IOF) (Ordas et al., 2003), a technique that replaces the Mahalanobis distance with feature selection from a set of optimal local features. The current model training for these studies has also been limited to mid-ventricular, end-diastolic images. The local search of corresponding points during ASM segmentation can be made more reliable by the use of a robust estimator, such as Robust Point Matching, a technique that allows to match two sets of features using thin-plate splines (Abi-Nahed et al., 2006). This method has been specifically applied to the RV segmentation.

Extension of the model to the temporal dimension is proposed in (Lelieveldt et al., 2001), with the introduction of 2D+time Active Appearance Motion

[3]Note that here the segmentation is performed in full-size image volumes. The location of the approximate center of the LV cavity is found with a Hough transform and is used to place the AAM model on the target image.

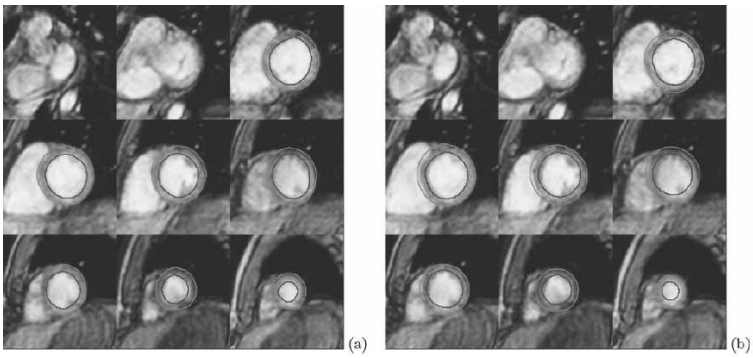

Figure 10: Segmentation results by 3D AAM. (a) Manually identified contours. (b) 3D AAM determined segmentation of the left ventricle (from (Mitchell et al., 2002), ©2002 IEEE)

Model (AAMM). Authors propose to extend the 2D AAM framework by considering the whole sequence of images over one cardiac cycle and by modeling not only shape and gray levels of the heart, but also its motion. Since the number of images per cardiac cycle varies from one patient to another (from 16 to 25 in their study), a temporal normalization is required, here set to 16 phases. The model allows to obtain in a fast manner segmentation over the whole cardiac cycle, still limited to mid-ventricular slice. The extension to 3D AAM and ASM is presented in (Mitchell et al., 2002; Stegmann and Pedersen, 2005; van Assen et al., 2006), although not straightforward, especially because the model requires point correspondences between shapes (Figure 10). The great amount of data to be processed in 3D models leads to an increase of the computational load, that can be lowered thanks to the use of techniques such as grid computing Ordas et al. (2005).

4.3.3. Atlas-guided segmentation and registration

An atlas describes the different structures present in a given type of image. It can be generated by manually segmenting an image or by integrating information from multiple segmented images from different individuals. Given an atlas, an image can be segmented by mapping its coordinate space to that of the atlas, using a registration process (Rohlfing et al., 2005). Widely applied to brain segmentation (Collins et al., 1995), this technique has also been used for heart segmentation. As shown in Figure 11, the principle is to register the labeled atlas onto the image to be segmented, and then apply the

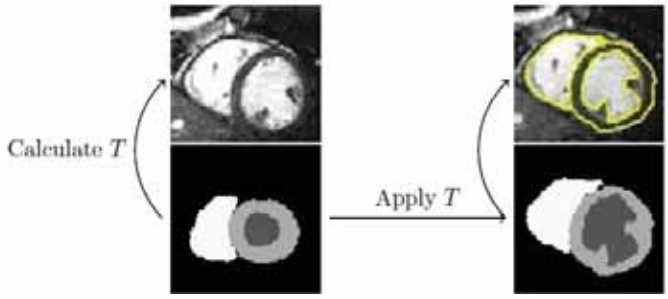

Figure 11: Anatomical atlas-based segmentation principle: (i) computation of the transformation T between the atlas and the image and (ii) deformation of the atlas by T (from (Lorenzo-Valdés et al., 2002), with kind permission from Springer Science+Business Media)

obtained transformation to the atlas, so as to obtain the final segmentation. Segmentation can thus easily be propagated throughout the cardiac cycle using the same principle.

In the literature, the construction of an anatomical heart atlas is based on the segmentation of a single images (Lorenzo-Valdés et al., 2002), an average segmentation result obtained over a population of healthy volunteers (14 (Lorenzo-Valdés et al., 2004) or 25 (Lötjönen et al., 2004)), or a cadaver atlas (Zhuang et al., 2008). The atlas or model can be matched on a new individual using non-rigid registration (NRR), a transformation that accounts for elastic deformations. NRR consists in maximizing a similarity measure between a source image S (the atlas) and a target or reference image R (the unsegmented image). Since the atlas and the MR image can have non corresponding gray levels, the similarity criterion must only account for statistical dependencies between them. The normalized mutual information measure E_{NMI}, widely used in NRR (Studholme et al., 1999), is based on individual and joint gray level distributions. It is defined as:

$$E_{NMI}(S,R) = \frac{H(S) + H(R)}{H(S,R)}$$

where $H(\cdot)$ denotes marginal entropy and $H(\cdot,\cdot)$ joint entropy of corresponding pixel or voxel pairs. Maximizing only the similarity criterion provides under-constrained equations, that makes image registration an ill-posed problem and thus requires the use of additional constraints. One way is to restrict

the transformation space to parametric transformations, such as cubic splines (Lorenzo-Valdés et al., 2002) or the basis of eigenshapes, obtained with a PCA on the database of shapes (Lötjönen et al., 2004). Another way is to add a regularization term to the similarity criterion, such as a classical viscous fluid model (Zhuang et al., 2008), or a statistical model (Lötjönen et al., 2004). In this latter work, the variability of the shape in the database of subjects is used as a regularizer. This variability is modeled with probabilistic shape models, including a probabilistic atlas, that provides the probability that a structure appears at each pixel. It is constructed by affinely registering all subjects to the reference, blurring the registered segmentation image with a Gaussian kernel and averaging all blurred segmentation. It has the advantage not to require point correspondence. Note also the use of a probabilistic atlas in (Lorenzo-Valdés et al., 2004), to initialize the parameters of an EM algorithm. The segmentation obtained after convergence of the EM algorithm is refined thanks to contextual spatial information modeled through Markov random fields.

4.3.4. Conclusion

By imposing constraints on the final contour through the use of a statistical model, strong prior based methods can overcome the previously defined segmentation problems (ill-defined cavity borders, presence of papillary muscles and gray level variations around the myocardium), without the need of user interaction, but at the expense of manually building a training set. The composition of the training set is questionable, as variability depend upon initial data. ASM cannot approximate data that are not in the training set and have to be representative enough of all possible heart shapes to achieve high accuracy. In (Zhang et al., 2010), the authors compensate the limited size of their training set by introducing manual segmentation of the first frame, thus improving the robustness of their method. Note that incorporation of time dimension and the third dimension into the model is not straightforward. For AAM, its high dimension increases the risk of overfitting. The non-rigid registration framework is more flexible, allowing for shapes not present in the training set, but does not impose anatomical constraint on the transformation. As a result, the composition of the atlas has little influence on the segmentation results, since it is only used as a starting point for registration (Zhuang et al., 2008).

5. Results and discussion

5.1. Methodological issues

Now let us examine how issues presented in Section 3.2 have been dealt with, according to the type of methods, by commenting Table 2. Among the 70 papers that have been reviewed in this paper, only three studies are entirely devoted to the RV, while a quarter of the rest of the papers show segmentation results on both ventricles. As mentioned above, physical characteristics of the RV as well as its lesser vital function has restrained research efforts on its segmentation. Nonetheless there is an increasing interest for the segmentation and volume computation of the RV, since MRI is increasingly used as a standard tool in the evaluation of RV function, being the most accurate tool for assessing RV volume (Haddad et al., 2008). Furthermore, in some pathologies (RV outflow tract obstruction, pulmonary stenosis, transposition of great vessels, tetralogy of Fallot, pulmonary hypertension), the RV is generally hypertrophied, which could help the segmentation process. Because of the RV's greatly varying shape, strong prior-based methods and in particular, atlas-based methods, thanks to their flexibility, seem of particular interest for RV segmentation. The endocardium and epicardium are of different nature, and thus present different segmentation challenges, as described in Section 2.2. For some categories of methods, namely image-driven methods and pixel-classification based approaches, specific solutions for each contour have been developed. On the contrary, model-based approaches do not require the design of two different algorithms. One of the segmentation challenges is the handling of papillary muscles. Currently, the common segmentation standards recommend to consider them as part as the ventricle cavity and to contour only the wall, because manual segmentation is more reproductible in this case, than when papillary muscles are segmented as well. But the exact cavity volume computation should exclude the volume occupied by the papillary muscles. Indeed, in some methods, pillars are segmented as well, authors arguing that the radiologist should decide whether to incorporate them or not (Pednekar et al., 2006; Lynch et al., 2006a).

Regarding the use of external information, this review highlights the fact that knowledge is necessarily integrated into the segmentation process, be it during the initialization phase (through user interaction) or during the process itself, with different prior levels. The tradeoff between user interaction

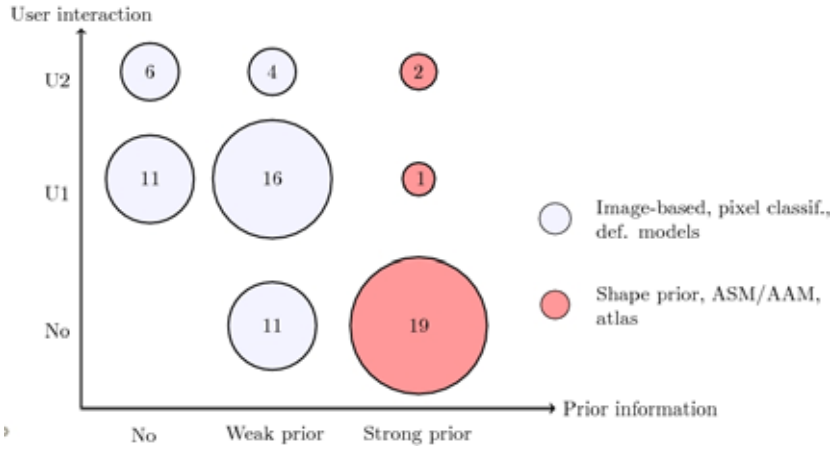

Figure 12: Levels of user interaction vs. levels of prior in cardiac MR segmentation methods in terms of paper numbers. Each circle is proportional to the number of concerned papers. U1: Limited user interaction. U2: Advanced user interaction. WP: Weak prior. SP: Strong prior.

levels and levels of external information is illustrated in Figure 12.

5.2. Tracking and motion information

Only a few methods really exploit information provided by cardiac motion, partly because of the complexity and the variability of the motion model, but also because ED and ES image segmentation are sufficient for estimating the cardiac contractile function in a clinical context. Making use of the temporal dimension can help the segmentation process and yields temporally consistent solutions. Moreover, it allows to segment the ventricle borders over a complete cardiac cycle and to investigate in more details on cardiac deformations and strain. Temporal continuity is also of interest for the clinician during manual segmentation, as he often examines images that follow or precede the image to be segmented in the sequence, as well as corresponding images in slices below or above. The expert behavior can thus be emulated by considering that the neighborhood of each voxel includes its six spatial nearest neighbours and the voxels in the neighbouring time frames of the sequence, such as in MRF (Lorenzo-Valdés et al., 2004) or in (Cousty et al., 2010), where a 4D graph corresponding to the 3D+t sequence is considered.

Tracking the ventricle contours over time may be performed with or without external knowledge. In this latter case, tracking relies on intrinsic properties of the segmentation methods. The variational approach of deformable models has been shown to be a very powerful and versatile framework for tracking the ventricle borders, the temporal resolution of cardiac MR allowing for using the segmentation result of the previous frame and propagating it to the next one (Pham et al., 2001; Gotardo et al., 2006; Hautvast et al., 2006; Ben Ayed et al., 2009). In order to improve the robustness of the propagation results, solutions have been proposed, like tracking the contours both backwards and forwards in time (Gotardo et al., 2006) and constraining the contour to respect the user's preference by maintaining it to a constant position, through the matching of gray level profiles (Hautvast et al., 2006). Non-rigid registration may also be used to propagate manually obtained contours or a heart atlas (Lorenzo-Valdés et al., 2002; Noble et al., 2003; Zhuang et al., 2008). In this case, the segmentation boils down to a registration problem: the transformation to match one (segmented) image to the other (unsegmented) is then applied to the contour of the segmented image. Segmentation and registration can also be coupled together by searching jointly for the epicardial and encocardial contours, and for an aligment transformation to a shape reference (Paragios et al., 2002).

Deformable models also are a good way to incorporate knowledge regarding heart motion. Prior knowledge about cardiac motion can be encoded in a weak manner, by temporally averaging the trajectories of the contour or surface points (Heiberg et al., 2005; Montagnat and Delingette, 2005), or in a strong manner, by using external knowledge. In (Lynch et al., 2008), the authors observed that the change of the blood volume of the ventricle is intrinsically linked to the boundary motion and that the volume decreases and increases during one cardiac cycle. The movement of the contour points are then modeled by an inverted Gaussian function, used to constrain the deformation of the level set. The dynamics of the heart can be taken into account via a biomechanical model (see Section 4.2.3), used not to predict motion but to regularize the deformation of the volumetric model, or by considering the moving boundaries as constituting a dynamic system, whose state must be estimated thanks to observations (the images) and a model, learned from training date (Sénégas et al., 2004; Sun et al., 2005). This explicit combination of shape and motion information, together with the appearance of the heart, can also be embedded in an ASM/AAM framework as a single shape

and intensity sample (Lelieveldt et al., 2001).

5.3. Assessment of segmentation accuracy

The assessment of segmentation accuracy greatly varies among reported works and ranges from visual qualitative assessment to perpendicular distance between contours computation, via surface overlap, ventricle volume, mass and EF computation. Note that almost all of the strong prior-based approaches are assessed via the mean P2C error. Test conditions change also a lot from one study to another: the number of test images, the number and nature of the patients (healthy and/or pathological), the phase of the cardiac cycle (only ED vs. all phases), the slice levels (only mid-ventricular level vs. all slice levels), not to forget that these conditions are sometimes not or only partly specified. Since these conditions have an influence on the segmentation complexity and thus on the final result, they have been reported in the results table (Table 3). The last lines of this table include the MICCAI'09 challenge studies[4]. In the MICCAI'09 contest, two databases (one for training and the other for validation) have been provided to the participants, and results are provided either on one or both databases. Interestingly, the methods that have been assessed during this challenge are quite representative of existing methods. They range from simple image-based techniques, as proposed in (Huang et al., 2009; Lu et al., 2009), to ASM and AAM (O'Brien et al., 2009; Wijnhout et al., 2009), including deformable models (Constantinides et al., 2009) (an improved version of (El Berbari et al., 2007)) and (Casta et al., 2009), taking over works from (Pham et al., 2001), a 4D watershed framework (Marak et al., 2009), based on (Cousty et al., 2007), and Jolly's image-based method (Jolly, 2009) based on (Jolly et al., 2009).

In order to limit the scope of our comparison, and also because it provides the best estimate of segmentation accuracy, the focus is given in this review to the mean distance between contours. The choice of mean P2C error allows for comparison with intra and inter-observer variability of manual contouring, which is in the range 1-2mm (Ordas et al., 2005; van Assen et al., 2006; Lötjönen et al., 2004; Marak et al., 2009). On the whole, reported errors compare favorably to this value. As expected, error is higher

[4]The database of the MICCAI'09 contest is the Sunnybrook Cardiac MR Database, available at `http://sourceforge.net/projects/cardiac-mr/files/`.

on the epicardial wall than on the endocardial one, a result that can be verified in almost all studies. Results obtained on ED images are also better than results obtained on other phases. Note that a few segmentation results, especially on the RV endocardium, have been obtained on a reduced number of slices, highlighting the difficulty of segmenting apical and basal images. In a restricted number of papers, the spatial distribution of errors is reported (Lin et al., 2006; Jolly et al., 2009; Grosgeorge et al., 2010). Results confirm that segmentation is more difficult in apical than in basal or mid-ventricular slices. Because testing conditions differ from one study to another, it seems difficult to draw more conclusions. Regarding the MICCAI Challenge studies, the ambiguity in the database choice does not allow for full comparison of the results. Nonetheless, one can note that among the eight tested methods, the ones that obtained the best results are image-based techniques (Lu et al., 2009; Huang et al., 2009). However these techniques require user interaction and cannot assess the ventricular surface in all phases, contrary to (O'Brien et al., 2009; Casta et al., 2009; Jolly, 2009). In this sense, the work described in (Jolly, 2009) offers a good compromise. Although results presented in (Lu et al., 2009; Huang et al., 2009; Constantinides et al., 2009) are interesting, their associated methodologies are LV specific and not applicable to the RV, whereas it would straightforwardly possible with more generic methodologies such as in (O'Brien et al., 2009; Wijnhout et al., 2009). These trends illustrates the compromise between method performance and specificity.

6. Conclusion and perspectives

This paper has been presenting segmentation methods in cardiac MRI. It seemed important to us to integrate the recent developments of the last decade about prior knowledge based segmentation, almost 10 years after Frangi et al.'s comprehensive review (Frangi et al., 2001). We have proposed a categorization for these methods, highlighting the key role of the type of prior information used during segmentation, and have distinguished three levels of information: (i) no information is used, but our study shows that in this case user interaction is required, (ii) weak prior, that is, low level information such as geometrical assumptions on the ventricle shape, often combined to low-level user interaction, (iii) strong prior such as statistical models, constructed or learned from a large number of manually segmented images, not requiring user interaction. Our image segmentation categoriza-

Table 3: Reported segmentation errors. H/P: number of healthy (H) and pathological (P) subjects. When multiple results were available, only best results were reported. [a]No standard deviation provided. [b]RMS error. [c]Leave-one-out protocol. [d]RV epicardium is taken into account for error computation. [e]Part of the MICCAI contest.

Authors	**Nb subj.**	**H/P**	**Slice nb.**	**Phases**	**Mean errors (mm)** LV epi	LV endo	RV endo
Mitchell et al. (2001)	20	11/9	3 mid	ED	1.75 ± 0.83[b]	1.71 ± 0.82[b]	2.46 ± 1.39[b]
Lelieveldt et al. (2001)	25[c]	-	3 mid	all	0.77 ± 0.74	0.63 ± 0.65	-
Mitchell et al. (2002)	56[c]	38/18	8-14	ED	2.63 ± 0.76	2.75 ± 0.86	-
Ordas et al. (2003)	74	13/61	3 mid	5 ph.	1.52 ± 2.01[d]	1.80 ± 1.74	1.20 ± 1.47
Kaus et al. (2004)	121	0/121	7-10	ED	2.62 ± 0.75	2.28 ± 0.93	-
				ES	2.92 ± 1.38	2.76 ± 1.02	-
Sénégas et al. (2004)	30	-	5	ED	1.98[a]	1.34[a]	-
				ES	2.74[a]	2.62[a]	-
Üzümcü et al. (2006)	20	2/18	8-12	all	1.77 ± 0.57	1.86 ± 0.59	-
Lynch et al. (2006a)	25	-	5-12	ED, ES	1.31 ± 1.86	0.69 ± 0.88	-
Lynch et al. (2006b)	4	-	-	all	1.83 ± 1.85	0.76 ± 1.09	-
van Assen et al. (2006)	15	15/0	10-12	ED	2.23 ± 0.46	1.97 ± 0.54	-
Abi-Nahed et al. (2006)	13	-	-	ED	-	-	1.1[a]
Lorenzo-V. et al (2004)	10	0/10	3 mid	all	2.99 ± 2.65	2.21 ± 2.22	2.89 ± 2.56
				ED	2.75 ± 2.62	1.88 ± 2.00	2.26 ± 2.13
Lötjönen et al. (2004)	25[c]	25/0	4-5	ED	2.77 ± 0.49[d]	2.01 ± 0.31	2.37 ± 0.5
Hautvast et al. (2006)	69	-	9/14	ES	1.84 ± 1.04	2.23 ± 1.10	2.02 ± 1.21
El Berbari et al. (2007)	13	-	3	ED	1.3 ± 0.7	0.6 ± 0.3	-
Jolly et al. (2009)	19	-	all	ED, ES	2.91[a,b]	2.48[a,b]	-
Zhang et al. (2010)	25	25/0	-	all	1.67 ± 0.3	1.81 ± 0.4	2.13 ± 0.39
	25	0/25	-	all	1.71 ± 0.45	1.97 ± 0.58	2.92 ± 0.73
Cousty et al. (2010)	18	0/18	9-14	ED, ES	1.42 ± 0.36	1.55 ± 0.23	-
Casta et al. (2009)[e]	15	3/12	6-12	ED, ES	2.72[a]	-	-
Wijnhout et al. (2009)[e]	15	3/12	6-12	ED, ES	2.29[a]	2.28[a]	-
Lu et al. (2009)[e]	15	3/12	6-12	ED, ES	2.07 ± 0.61	1.91 ± 0.63	-
Marak et al. (2009)[e]	-	-	6-12	ED, ES	3 ± 0.59	2.6 ± 0.38	-
Constantinides et al. (2009)[e]	30	6/24	6-12	ED, ES	2.04 ± 0.47	2.35 ± 0.57	-
Jolly (2009)[e]	30	6/24	6-12	ED, ES	2.26 ± 0.59	1.97 ± 0.48	-
Huang et al. (2009)[e]	30	6/24	6-12	ED, ES	2.06 ± 0.39	2.11 ± 0.41	-
O'Brien et al. (2009)[e]	30	6/24	6-12	ED, ES	3.73[a]	3.16[a]	-

tion includes on the one hand image-driven and pixel classification based approaches, and deformable models, making use of weak or no prior. On the other hand, strong prior approaches comprise shape prior deformable models, ASM and AAM, and atlas-based segmentation. We have tried to point out that segmentation results on cardiac images have been obtained in diverse experimental conditions, on different, private image databases and using varying error measures, thus making it difficult to conclude on the efficiency or the superiority of one method over the others. One result of our review is that segmentation results are generally satisfying for the LV, especially on mid-ventricular slices, since the precision is of the order of manual

tracing variability. These results are suitable for clinical pratice and finally show that room for improvement on the LV segmentation problem might be limited and restricted to basal and apical slices. On the other hand, although comparable to LV results, the RV segmentation results have been reported in a limited number of papers. This task is still a critical issue, due to the varying and complex shape of this ventricle and to its thin and ill-defined borders, appearing fuzzy in apical slices.

Other challenging image processing and pattern recognition issues connected to short axis MR images include the automatic identification of ED and ES frames, currently made by browsing through all the image sequence (Lalande et al., 2004). Another topic is the determination of imaging slices that can be taken into account for volume computation. Physicians are confronted to a hard choice for those situated around the base of the heart, since certain slices are above the ventricle and include atria.

Until now, the problem of LV segmentation was still open, partly because of the lack of publicly available image database and of common performance evaluation protocols. Today, such an image database, initially made available during the MICCAI'09 contest, exists and should be used to assess and compare further proposed algorithms, along with the proposed validation tools, namely the mean perpendicular distance between contours, and the Dice metric (surface overlap). An equivalent database of segmented images would be of great help for RV segmentation, especially because of the growing interest for this very challenging segmentation task.

References

Abi-Nahed, J., Jolly, M.-P., Yang, G.-Z., 2006. Robust active shape models: A robust, generic and simple automatic segmentation tool. In: Proc. of Medical Image Computing and Computer-Assisted Intervention (MICCAI). No. 2. pp. 1–8.

Allender, S., Scarborough, P., Peto, V., Rayner, M., Leal, J., Luengo-Fernandez, R., Gray, A., 2008. European cardiovascular disease statistics. European Heart Network.

Battani, R., Corsi, C., Sarti, A., Lamberti, C., Piva, T., Fattori, R., 2003. Estimation of right ventricular volume without geometrical assumptions

utilizing cardiac magnetic resonance data. In: Computers in Cardiology. pp. 81–84.

Ben Ayed, I., Li, S., Ross, I., 2009. Embedding overlap priors in variational left ventricle tracking. IEEE Trans. Med. Imag. 28 (12), 1902–1913.

Billet, F., Sermesant, M., Delingette, H., Ayache, N., 2008. Cardiac motion recovery by coupling an electromechanical model and cine-MRI data: First steps. In: Proc. of the Workshop on Computational Biomechanics for Medicine III (Workshop MICCAI).

Billet, F., Sermesant, M., Delingette, H., Ayache, N., 2009. Cardiac motion recovery and boundary conditions estimation by coupling an electromechanical model and cine-MRI data. In: Proc. of Functional Imaging and Modeling of the Heart (FIMH). Vol. 5528 of LNCS. pp. 376–385.

Bland, J., Altman, D., 1986. Statistical methods for assessing agreement between two methods of clinical measurement. Lancet 1 (8476), 307–310.

Boudraa, A.-E.-O., 1997. Automated detection of the left ventricular region in magnetic resonance images by fuzzy C-means model. Int J Card Imaging 13 (4), 347–355.

Caselles, V., Catte, F., Coll, T., Dibos, F., 1993. A geometric model for active contours. Numerische Mathematik 66, 1–31.

Cassen, C., Domenger, J., Braquelaire, J., Barat, J., 2001. Left ventricular segmentation in MRI images. In: Proceedings of the 2nd International Symposium on Image and Signal Processing and Analysis (ISPA). Pula, Croatia, pp. 244–249.

Casta, C., Clarysse, P., Schaerer, J., Pousin, J., 2009. Evaluation of the Dynamic Deformable Elastic Template model for the segmentation of the heart in MRI sequences. In: MICCAI 2009 Workshop on Cardiac MR Left Ventricle Segmentation Challenge. MIDAS Journal.

Caudron, J., Fares, J., Bauer, F., Dacher, J.-N., 2011. Left ventricular diastolic function assessment by cardiac MRI. RadioGraphics in press.

Chakraborty, A., Staib, L., Duncan, J., 1996. Deformable boundary finding in medical images by integrating gradient and region information. IEEE Trans. Med. Imag. 15, 859–870.

Cocosco, C., Netsch, T., Senegas, J., Bystrov, D., Niessen, W., Viergever, M., 2004. Automatic cardiac region-of-interest computation in cine 3D structural MRI. In: Proc. of the Conference on Computer Assisted Radiology and Surgery (CARS). Chicago, pp. 1126–1131.

Cocosco, C., Wiro, W. N., Netsch, T., Vonken, E.-J., Lund, G., Stork, A., Viergever, M., 2008. Automatic image-driven segmentation of the ventricles in cardiac cine MRI. J Magn Reson Imaging 28 (2), 366–74.

Collins, D., Holmes, C., Peters, T., Evans, C., 1995. Automatic 3-D model-based neuroanatomical segmentation. Human brain mapping 3 (3), 190–208.

Constantinides, C., Chenoune, Y., Kachenoura, N., Roullot, E., Mousseaux, E., Herment, A., Frouin, F., 2009. Semi-automated cardiac segmentation on cine magnetic resonance images using GVF-Snake deformable models. In: MICCAI 2009 Workshop on Cardiac MR Left Ventricle Segmentation Challenge. MIDAS Journal.

Cootes, T., Cooper, D., Taylor, C., Graham, J., 1995. Active shape models - their training and application. Computer Vision and Image Understanding 61 (1), 38–59.

Cootes, T., Edwards, G., Taylor, C., 1998. Interpreting face images using active appearance models. In: In Proc. European Conf. on Computer Vision. 2. pp. 484–498.

Cousty, J., Najman, L., Couprie, M., Clment-Guinaudeau, S., Goissen, T., Garot, J., 2007. Automated, accurate and fast segmentation of 4D cardiac MR images. In: Proc. of Functional Imaging and Modeling of the Heart (FIMH). Vol. 4466 of LNCS. pp. 474–483.

Cousty, J., Najman, L., Couprie, M., Clment-Guinaudeau, S., Goissen, T., Garot, J., 2010. Segmentation of 4D cardiac MRI: automated method based on spatio-temporal watershed cuts. Image and Vision Computing 28, 1229–1243.

Cremers, D., Rousson, M., Deriche, R., 2007. A review of statistical approaches to level set segmentation: Integrating color, texture, motion and shape. International Journal of Computer Vision 72 (2), 195–215.

Dawant, B., Zijdenbos, A., 2000. Image segmentation. In: Sonka, M., Fitzpatrick, J. (Eds.), Handbook of Medical Imaging. Vol. 2. SPIE Press, Bellingham, WA, pp. 71–127.

Dempster, A., Laird, N., Rubin, D., 1977. Maximum likelihood from incomplete data via the EM algorithm. Journal of the Royal Statistical Society 39 (1), 1–38.

El Berbari, R., Bloch, I., Redheuil, A., Angelini, E., Mousseaux, E., Frouin, F., Herment, A., 2007. An automated myocardial segmentation in cardiac MRI. In: Conf Proc IEEE Eng Med Biol Soc. pp. 4508–4511.

François, C., Fieno, D., Shors, S., Finn, P., 2004. Left ventricular mass: Manual and automatic segmentation of true FISP and FLASH cine MR images in dogs and pigs. Radiology 230, 389–395.

Frangi, A., D.Rueckert, Schnabel, J., Niessen, W., 2002. Automatic construction of multiple-object three-dimensional statistical shape models: Application to cardiac modeling. IEEE Trans. Med. Imag. 21 (9), 1151–1166.

Frangi, A., Niessen, W., Viergever, M., 2001. Three-dimensional modeling for functional analysis of cardiac images: A review. IEEE Trans. Med. Imaging 20 (1).

Fu, J., Chai, J., Wong, S., 2000. Wavelet-based enhancement and detection of left ventricular endocardial and epicardial boundaries in magnetic resonance images. Magn. Reson. Imaging 18, 1135–1141.

Geiger, D., Gupta, A., Costa, L., Vlontzos, J., 1995. Dynamic programming for detecting, tracking and matching deformable contours. IEEE Trans. Pattern Anal. Machine Intell. 19 (6), 294–302.

Gering, D., 2003. Automatic segmentation of cardiac MRI. In: Proc. of Medical Image Computing and Computer-Assisted Intervention (MICCAI). No. 1 in LNCS. pp. 524–532.

Goshtasby, A., Turner, D., 1995. Segmentation of cardiac cine MR images for extraction of right and left ventricular chambers. IEEE Trans. Med. Imag. 14 (1), 56–64.

Gotardo, P., Boyer, K., Saltz, J., Raman, S., 2006. A new deformable model for boundary tracking in cardiac MRI and its application to the detection of intra-ventricular dyssynchrony. In: IEEE Computer Society Conference on Computer Vision and Pattern Recognition - Volume 1 (CVPR'06). pp. 736–743.

Grosgeorge, D., Petitjean, C., Caudron, J., Fares, J., Dacher, J.-N., 2010. Automatic cardiac ventricle segmentation in MR images: a validation study. International Journal of Computer Assisted Radiology and Surgery, DOI 10.1007/s11548–010–0532–6, in press.

Gupta, A., von Kurowski, L., Singh, A., Geiger, D., Liang, C.-C., Chiu, M.-Y., Adler, L., Haacke, M., Wilson, D., 1993. Cardiac MR image segmentation using deformable models. In: Computers in Cardiology. London, UK, pp. 747–750.

Haddad, F., Hunt, S., Rosenthal, D., Murphy, D., 2008. Right Ventricular Function in Cardiovascular Disease, Part I - Anatomy, Physiology, Aging, and Functional Assessment of the Right Ventricle. Circulation 117, 1436–1448.

Hautvast, G., Lobregt, S., Breeuwer, M., Gerritsen, F., 2006. Automatic contour propagation in cine cardiac magnetic resonance images. IEEE Trans. Med. Imag. 25 (11), 1472 – 1482.

Heiberg, E., Sjögren, J., Ugander, M., Carlsson, M., Engblom, H., Arheden, H., 2010. Design and validation of Segment - a freely available software for cardiovascular image analysis. BMC Medical Imaging 10, 1.

Heiberg, E., Wigström, L., Carlsson, M., Bolger, A., Karlsson, M., 2005. Time resolved three-dimensional segmentation of the left ventricle. In: Proceedings of IEEE Computers In Cardiology. No. 32. Lyon, France, pp. 599–602.

Heimann, T., Meinzer, H.-P., 2009. Statistical shape models for 3D medical image segmentation: A review. Medical Image Analysis 13 (4), 543–563.

Huang, J., Huang, X., Metaxas, D., Axel, L., 2007. Dynamic Texture based Heart Localization and Segmentation in 4-D Cardiac Images. In: Proc. of the IEEE Intl Symposium on Biomedical Imaging: From Nano to Macro (ISBI). pp. 852–855.

Huang, S., Liu, J., Lee, L., Venkatesh, S., Teo, L., Au, C., Nowinski, W., 2009. Segmentation of the Left Ventricle from Cine MR Images Using a Comprehensive Approach. In: MICCAI 2009 Workshop on Cardiac MR Left Ventricle Segmentation Challenge. MIDAS Journal.

Jolly, M.-P., 2006. Automatic segmentation of the left ventricle in cardiac MR and CT images. International Journal of Computer Vision 70 (2), 151–163.

Jolly, M.-P., 2008. Automatic recovery of the left ventricular blood pool in cardiac cine MR images. In: Proc. of Medical Image Computing and Computer-Assisted Intervention (MICCAI). LNCS 5241. pp. 110–118.

Jolly, M.-P., 2009. Fully Automatic Left Ventricle Segmentation in Cardiac Cine MR Images Using Registration and Minimum Surfaces. In: MICCAI 2009 Workshop on Cardiac MR Left Ventricle Segmentation Challenge. MIDAS Journal.

Jolly, M.-P., Duta, N., Funka-Lea, G., 2001. Segmentation of the left ventricle in cardiac MR images. In: Proceedings of the Eighth IEEE International Conference on Computer Vision, ICCV 2001. No. 1. Vancouver, BC, Canada, pp. 501–508.

Jolly, M.-P., Xue, H., Grady, L., J., Gühring, 2009. Combining registration and minimum surfaces for the segmentation of the left ventricle in cardiac cine MR images. In: Proc. of Medical Image Computing and Computer-Assisted Intervention (MICCAI). LNCS 5762. pp. 910–918.

Kass, M., Witkin, A., Terzopoulos, D., 1988. Snakes: Active contour models. International Journal of Computer Vision 1, 321–332.

Katouzian, A., Konofagou, E., Prakash, A., 2006. A new automated technique for left-and right-ventricular segmentation in magnetic resonance imaging. In: Conf Proc IEEE Eng Med Biol Soc. Vol. 1. pp. 3074–3077.

Kaus, M., von Berg, J., Weese, J., Niessen, W., Pekar, V., 2004. Automated segmentation of the left ventricle in cardiac MRI. Medical Image Analysis 8 (3), 245–254.

Kaushikkar, S., Li, D., Haale, E., Dávila-Román, V., 1996. Adaptive blood pool segmentation in three-dimensions: application to MR cardiac evaluation. J Magn Reson Imaging 6, 690–697.

Kedenburg, G., Cocosco, C., Köthe, U., Niessen, W., Vonken, E., Viergever, M., 2006. Automatic cardiac MRI myocardium segmentation using graph-cut. In: Proceedings of SPIE. No. 6144 in Medical Imaging.

Lalande, A., Legrand, L., Walker, P., Guy, F., Cottin, Y., Roy, S., Brunotte, F., 1999. Automatic detection of left ventricular contours from cardiac cine magnetic resonance imaging using fuzzy logic. Investigative Radiology 34 (3), 211–217.

Lalande, A., Salvé, N., Comte, A., Jaulent, M.-C., Legrand, L., Walker, P., Cottin, Y., Wolf, J., Brunotte, F., 2004. Left ventricular ejection fraction calculation from automatically selected and processed diastolic and systolic frames in short-axis cine-MRI. Journal of Cardiovascular Magnetic Resonance 6 (4), 817–827.

Lee, H., Codella, N., Cham, M., Prince, M., Weinsaft, J., Wang, Y., 2008. Left ventricle segmentation using graph searching on intensity and gradient and a priori knowledge (lvGIGA) for short-axis cardiac magnetic resonance imaging. J Magn Reson Imaging 28 (6), 1393–401.

Lelieveldt, B., Mitchell, S., Bosch, J., van der Geest, R., Sonka, M., Reiber, J., 2001. Time-continuous segmentation of cardiac image sequences using active appearance motion models. In: Information Processing in Medical Imaging: 17th International Conference (IPMI). LNCS. Davis, CA, USA, p. 446.

Lin, X., Cowan, B., Young, A., 2005. Model-based graph cut method for segmentation of the left ventricle. In: IEEE International Conference of the Engineering in Medicine and Biology Society (EMBS). pp. 3059–3062.

Lin, X., Cowan, R., Young, A., 2006. Automated detection of left ventricle in 4D MR images: experience from a large study. In: Proc. of Medical Image Computing and Computer-Assisted Intervention (MICCAI). No. 9 in LNCS. pp. 728–35.

Liu, N., Strugnell, W., Slaughter, R., Riley, R., Crozier, S., Wilson, S., Liu, F., Appleton, B., Trakic, A., Wei, Q., 2005. Right ventricle extraction by low level and model-based algorithm. In: Proceedings of the IEEE Engineering in Medicine and Biology society (EMBS). pp. 1607–1610.

Lloyd-Jones, D., 2010. Heart Disease and Stroke Statistics–2010 Update. American Heart Association.

Lorenzo-Valdés, M., Sanchez-Ortiz, G., Elkington, A., Mohiaddin, R., Rueckert, D., 2004. Segmentation of 4D cardiac MR images using a probabilistic atlas and the EM algorithm. Medical Image Analysis 8 (3), 255–265.

Lorenzo-Valdés, M., Sanchez-Ortiz, G., Mohiaddin, R., Rueckert, D., 2002. Atlas-based segmentation and tracking of 3D cardiac MR images using non-rigid registration. In: Proc. of Medical Image Computing and Computer-Assisted Intervention (MICCAI). LNCS. Tokyo, Japan, pp. 642–650.

Lötjönen, J., Kivistö, S., Koikkalainen, J., Smutek, D., Lauerma, K., 2004. Statistical shape model of atria, ventricles and epicardium from short- and long-axis MR images. Medical Image Analysis 8 (3), 371–386.

Lu, Y., Radau, P., Connelly, K., Dick, A., Wright, G., 2009. Automatic image-driven segmentation of left ventricle in cardiac cine MRI. In: MICCAI 2009 Workshop on Cardiac MR Left Ventricle Segmentation Challenge. MIDAS Journal.

Lynch, M., Ghita, O., Whelan, P., 2006a. Automatic segmentation of the left ventricle cavity and myocardium in MRI data. Comput Biol Med 36 (4), 389–407.

Lynch, M., Ghita, O., Whelan, P., 2006b. Left-ventricle myocardium segmentation using a coupled level-set with a priori knowledge. Computerized Medical Imaging and Graphics 30 (4), 255–262.

Lynch, M., Ghita, O., Whelan, P., 2008. Segmentation of the left ventricle of the heart in 3D+t MRI data using an optimised non-rigid temporal model. IEEE Trans. Med. Imag. 27 (2), 195–203.

Mahnken, A., Mühlenbruch, G., Koos, R., Stanzel, S., Busch, P., Niethammer, M., Günther, R., Wildberger, J., 2006. Automated vs. manual assessment of left ventricular function in cardiac multidetector row computed tomography: comparison with magnetic resonance imaging. Journal European Radiology 16 (7), 1416–1423.

Marak, L., Cousty, J., Najman, L., Talbot, H., 2009. 4D Morphological segmentation and the MICCAI LV-segmentation grand challenge. In: MICCAI 2009 Workshop on Cardiac MR Left Ventricle Segmentation Challenge. MIDAS Journal.

Mitchell, S., Bosch, J., Lelieveldt, B., van der Geest, R., Reiber, J., Sonka, M., 2002. 3-D active appearance models: segmentation of cardiac MR and ultrasound images. IEEE Trans. Med. Imag. 21 (9), 1167–1178.

Mitchell, S., Lelieveldt, B., van der Geest, R., Bosch, J., Reiber, J., Sonka, M., 2000. Segmentation of cardiac MR images: An active appearance model approach. In: Proceedings of SPIE. No. 3979 in Medical Imaging. pp. 224–234.

Mitchell, S., Lelieveldt, B., van der Geest, R., Bosch, J., Reiber, J., Sonka, M., 2001. Multistage hybrid active appearance model matching: segmentation of left and right ventricles in cardiac MR images. IEEE Trans. Med. Imag. 20 (5), 415–423.

Montagnat, J., Delingette, H., 2005. 4D deformable models with temporal constraints: application to 4D cardiac image segmentation. Medical Image Analysis 9 (1), 87–100.

Nachtomy, E., Cooperstein, R., Vaturi, M., Bosak, E., Vered, Z., Akselrod, S., 1998. Automatic assessment of cardiac function from short-axis MRI: procedure and clinical evaluation. Magn. Reson. Imaging 16, 365–376.

Noble, N., Hill, D., Breeuwer, M., Schnabel, J., Hawkes, D., Gerritsen, F., Razavi, R., 2003. Myocardial delineation via registration in a polar coordinate system. Academic Radiology 10 (12), 1349–1358.

O'Brien, S., Ghita, O., Whelan, P., 2009. Segmenting the Left Ventricle in 3D Using a Coupled ASM and a Learned Non-Rigid Spatial Model. In: MICCAI 2009 Workshop on Cardiac MR Left Ventricle Segmentation Challenge. MIDAS Journal.

O'Donnell, T., Funka-Lea, G., Tek, H., Jolly, M.-P., Rasch, M., 2006. Comprehensive cardiovascular image analysis using MR and CT at Siemens Corporate Research. International Journal of Computer Vision 70 (2), 165–178.

Ordas, S., Boisrobert, L., Huguet, M., Frangi, A., 2003. Active shape models with invariant optimal features (IOF-ASM) - application to cardiac MRI segmentation. In: Computers in cardiology. No. 30. pp. 633–636.

Ordas, S., van Assen, H., Boisrobert, L., Laucelli, M., Puente, J., Lelieveldt, B., Frangi, A., 2005. Statistical modeling and segmentation in cardiac MRI using a grid computing approach. In: Advances in Grid Computing - EGC 2005. LNCS. pp. 6–15.

Osher, S., Sethian, J., 1988. Fronts propagating with curvature-dependent speed: Algorithms based on hamiltonjacobi formulation. J. Comput. Phys. 79, 12–49.

Otsu, N., 1979. A threshold selection method for gray-level histograms. IEEE Trans. Syst. Man Cybernet 1, 62–66.

Papademetris, X., Sinusas, A., Dione, D., Constable, R., Duncan, J., 2002. Estimating 3D left ventricular deformation from 3D medical image sequences using biomechanical models. IEEE Trans. Med. Imag. 21 (7), 786 – 800.

Paragios, N., 2002. A variational approach for the segmentation of the left ventricle in cardiac image analysis. International Journal of Computer Vision 50 (3), 345–362.

Paragios, N., Rousson, M., Ramesh, V., 2002. Knowledge-based registration and segmentation of the left ventricle: A level set approach. In: Applications of Computer Vision, 2002. (WACV 2002). Proceedings. Sixth IEEE Workshop on. pp. 37–42.

Pavani, S.-K., Delgado, D., Frangi, A., 2010. Haar-like features with optimally weighted rectangles for rapid object detection. Pattern Recognition 43 (1), 160–172.

Pednekar, A., Kurkure, U., Muthupillai, R., Flamm, S., 2006. Automated left ventricular segmentation in cardiac MRI. IEEE Trans Biomed Eng 53 (7), 1425–1428.

Pham, D., Xu, C., Prince, J., 2000. Current methods in medical image segmentation. Annual Review of Biomedical Engineering, Annual Reviews 2, 315–337.

Pham, Q., Vincent, F., Clarysse, P., Croisille, P., Magnin, I., 2001. A FEM-based deformable model for the 3D segmentation and tracking of the heart in cardiac MRI. In: Proceedings of the 2nd International Symposium on Image and Signal Processing and Analysis (ISPA). Pula, Croatia, pp. 250–254.

Pluempitiwiriyawej, C., Moura, J., Wu, Y., Ho, C., 2005. STACS: New active contour scheme for cardiac MR image segmentation. IEEE Trans. Med. Imag. 24 (5), 593–603.

Ranganath, S., 1995. Contour extraction from cardiac MRI studies using snakes. IEEE Trans. Med. Imag. 14 (2), 328–338.

Rohlfing, T., Brandt, R., Menzel, R., Russakoff, D., Maurer, C., 2005. Quo vadis, atlas-based segmentation ? In: The Handbook of Medical Image Analysis: Segmentation and Registration Models. Kluwer, Ch. 11.

Rougon, N., Petitjean, C., Cluzel, P., Prêteux, F., Grenier, P., 2005. A non rigid registration approach for quantifying myocardial contraction in tagged MRI using generalized information measures. Medical Image Analysis 9 (4), 353–375.

Santarelli, M., Positano, V., Michelassi, C., Lombardi, M., Landini, L., 2003. Automated cardiac MR image segmentation: theory and measurement evaluation. Medical Engineering and Physics 25 (2), 149–159.

Sénégas, J., Cocosco, C., Netsch, T., 2004. Model-based segmentation of cardiac MRI cine sequences: a bayesian formulation. In: Fitzpatrick, J., Sonka, M. (Eds.), Proceedings of SPIE. No. 5370 in Medical Imaging. pp. 432–443.

Sermesant, M., Forest, C., Pennec, X., Delingette, H., Ayache, N., 2003. Deformable biomechanical models: Application to 4D cardiac image analysis. Medical Image Analysis 7 (4), 475–488.

Sermesant, M., Moireau, P., Camara, O., Sainte-Marie, J., Andriantsimiavona, R., Cimrman, R., Hill, D. L., Chapelle, D., Razavi, R., 2006. Cardiac function estimation from mri using a heart model and data assimilation: Advances and difficulties. Medical Image Analysis 10 (4), 642 – 656.

Shors, S., Fung, C., François, C., Finn, P., Fieno, D., 2004. Accurate quantification of right ventricular mass at MR imaging by using cine true fast imaging with steady-state precession: study in dogs. Radiology 230 (2), 383–388.

Staib, L., Duncan, J., 1992. Boundary finding with parametrically deformable models. IEEE Trans. Pattern Anal. Machine Intell. 14 (11), 1061–1075.

Stalidis, G., Maglaveras, N., Efstratiadis, S., Dimitriadis, A., Pappas, C., 2002. Model-based processing scheme for quantitative 4-D cardiac MRI analysis. IEEE Trans Inf Technol Biomed. 6 (1), 59–72.

Stegmann, M., Nilsson, J., Grönning, B., 2001. Automated segmentation of cardiac magnetic resonance images. In: Proc. Intl. Soc. Mag. Reson. Med. 9. p. 827.

Stegmann, M., Pedersen, D., 2005. Bi-temporal 3D active appearance models with applications to unsupervised ejection fraction estimation. In: International Symposium on Medical Imaging 2005, San Diego, CA, Proc. of SPIE. Vol. 5747. pp. 336–350.

Studholme, C., Hill, D., Hawkes, D., 1999. An overlap invariant entropy measure of 3D medical image alignment. Pattern Recognition 32 (1), 71–86.

Sun, W., Cetin, M., Chan, R., Reddy, V., Holmvang, G., Chandar, V., Willsky, A., 2005. Segmenting and tracking the left ventricle by learning the dynamics in cardiac images. In: Proc. of the Information Processing in Medical Imaging Conference (IPMI). pp. 553–565.

Suri, J., 2000. Computer vision, pattern recognition and image processing in left ventricle segmentation: The last 50 years. Pattern Analysis and Applications 3 (3), 209–242.

Suri, J., Singh, S., Setarehdan, S., Sharma, R., Bovis, K., Comaniciu, D., Reden, L., 2001. A note on future research in segmentation techniques applied to neurology, cardiology, mammography and pathology. In: Advanced algorithmic approaches to medical image segmentation: state-of-the-art application in cardiology, neurology, mammography and pathology. Springer-Verlag New York, Inc., pp. 559–572.

Tsai, A., Yezzi, A., Wells, W., Tempany, C., Tucker, D., Fan, A., Grimson, W., Willsky, A., 2003. A shape-based approach to the segmentation of medical imagery using level sets. IEEE Trans. Med. Imag. 22 (2), 137–154.

Üzümcü, M., Frangi, A., Sonka, M., Reiber, J., Lelieveldt, B., 2003. ICA vs. PCA active appearance models: Application to cardiac MR segmentation. In: Proc. of Medical Image Computing and Computer-Assisted Intervention (MICCAI). pp. 451–458.

Üzümcü, M., van der Geest, R., Swingen, C., Reiber, J., Lelieveldt, B., 2006. Time continuous tracking and segmentation of cardiovascular magnetic resonance images using multidimensional dynamic programming. Investigative Radiology 41 (1), 52–62.

van Assen, H., Danilouchkine, M., Frangi, A., Ordas, S., Westenberg, J., Reiber, J., Lelieveldt, B., 2006. SPASM: A 3D-ASM for segmentation of sparse and arbitrarily oriented cardiac MRI data. Medical Image Analysis 10 (2), 286–303.

van der Geest, R., Jansen, E., Buller, V., Reiber, J., 1994. Automated detection of left ventricular epi- and endocardial contours in short-axis MR images. In: Computers in Cardiology. Bethesda, MD, USA, pp. 33–36.

Viola, P., Jones, M., 2001. Rapid object detection using a boosted cascade of simple features. In: Proceedings of IEEE Conference on Computer Vision and Pattern Recognition. pp. 511–518.

Waiter, G., McKiddie, F., Redpath, T., Semple, S., Trent, R., 1999. Determination of normal regional left ventricular function from cine-MR images using a semi-automated edge detection method. Magn. Reson. Imaging 17 (1), 99–107.

Wang, Y., Jia, Y., 2006. Segmentation of the left ventricle from cardiac MR images based on degenerated minimal surface diffusion and shape priors. In: Proc. of the 18th International Conference on Pattern Recognition (ICPR). No. 4. pp. 671–674.

Weng, J., Singh, A., Chiu, M., 1997. Learning-based ventricle detection from cardiac MR and CT images. IEEE Trans. Med. Imag. 16 (4), 378–391.

Wijnhout, J., Hendriksen, D., Assen, H. V., der Geest, R. V., 2009. LV Challenge LKEB Contribution: Fully Automated Myocardial Contour Detection. In: MICCAI 2009 Workshop on Cardiac MR Left Ventricle Segmentation Challenge. MIDAS Journal.

Xu, C., Pham, D. L., Prince, J. L., 2000. Medical image segmentation using deformable models. In: Handbook of Medical Imaging – Volume 2: Medical Image Processing and Analysis. SPIE Press, pp. 129–174.

Xu, C., Prince, J., 1998. Snakes, shapes, and gradient vector flow. IEEE Transactions on Image Processing 7 (3), 359 – 369.

Yan, P., Sinusas, A., Duncan, J. S., 2007. Boundary element method-based regularization for recovering of LV deformation. Medical Image Analysis 11 (6), 540 – 554.

Yeh, J., Fua, J., Wua, C., Lina, H., Chaib, J., 2005. Myocardial border detection by branch-and-bound dynamic programming in magnetic resonance images. Computer Methods and Programs in Biomedicine 79 (1), 19–29.

Yezzi, A., Kichenassamy, S., Kumar, A., Olver, P., Tannenbaum, A., 1997. A geometric snake model for segmentation of medical imagery. IEEE Trans. Med. Imag. 16 (2), 199–209.

Zambal, S., Hladuvka, J., Bühler, K., 2006. Improving segmentation of the left ventricle using a two-component statistical model. In: Proc. of Medical Image Computing and Computer-Assisted Intervention (MICCAI). LNCS. pp. 151–158.

Zhang, H., Wahle, A., Johnson, R., Scholz, T., Sonka, M., 2010. 4-D cardiac MR image analysis: Left and right ventricular morphology and function. IEEE Trans. Med. Imag. 29 (2), 350 – 364.

Zhuang, X., Hawkes, D., Crum, W., Boubertakh, R., Uribe, S., Atkinson, D., Batchelor, P., Schaeffter, T., Razavi, R., Hill, D., 2008. Robust registration between cardiac MRI images and atlas for segmentation propagation. In: Society of Photo-Optical Instrumentation Engineers (SPIE) Conference. p. 691408.

Zhukov, L., Bao, J., Guskov, I., Wood, J., Breen, D., 2002. Dynamic deformable models for 3D MRI heart segmentation. In: Proceedings of SPIE. Medical Imaging. pp. 1398–1405.